

## Structural transition in cold-compressed glassy carbon

HPSTAR  
736-2019Zhidan Zeng,<sup>1,\*</sup> Hongwei Sheng,<sup>1</sup> Liuxiang Yang,<sup>1</sup> Hongbo Lou,<sup>1</sup> Lijie Tan,<sup>1,2</sup> Vitali B. Prakapenka,<sup>3</sup> Eran Greenberg,<sup>3</sup> and Qiaoshi Zeng<sup>1,4</sup><sup>1</sup>Center for High Pressure Science and Technology Advanced Research (HPSTAR), Shanghai 201203, China<sup>2</sup>Institute of Atomic and Molecular Physics, Sichuan University, Chengdu 610065, China<sup>3</sup>Center for Advanced Radiation Sources, University of Chicago, Chicago, Illinois 60637, USA<sup>4</sup>Jiangsu Key Laboratory of Advanced Metallic Materials, School of Materials Science and Engineering, Southeast University, Nanjing 211189, People's Republic of China

(Received 27 October 2018; revised manuscript received 13 February 2019; published 27 March 2019)

Glassy carbon (GC) distinguishes itself from other carbon materials by its unique atomic structure and properties. Cold-compressed GC gives rise to new physical properties; however, the atomistic mechanism for the transitions remains elusive. In this study, by combining *in situ* high-pressure x-ray diffraction with first-principles calculations, we observe pressure-induced disappearance of the initial intermediate range order of GC, followed by formation of local tetrahedral structural domains and  $sp^3$  bonds. Correspondingly, the resistance of GC increases by four orders of magnitude during compression from  $\sim 20$  to  $\sim 61$  GPa. Both the structural and resistance transitions are partially reversible upon decompression, with noticeable hysteresis. Our results highlight the central role of layer distortions in inducing the  $sp^2$ -to- $sp^3$  bonding transition and provide the structural underpinning for the various transitions observed in cold-compressed glassy carbon.

DOI: [10.1103/PhysRevMaterials.3.033608](https://doi.org/10.1103/PhysRevMaterials.3.033608)

## I. INTRODUCTION

Carbon has numerous allotropes with diverse structure and associated properties owing to its flexibility in bonding (pure  $sp^1$ -,  $sp^2$ -, and  $sp^3$ -hybridized bonds, or combinations thereof). Glassy carbon (GC) is an amorphous carbon allotrope consisting primarily of  $sp^2$  bonds. GC possesses extraordinary properties such as very high thermal stability, extreme resistance to chemical attack, superelasticity, and high impermeability to gases; hence it has broad industrial applications [1–4]. Besides its technical importance, as an isotropic, highly disordered  $sp^2$ -bonded bulk carbon allotrope [5], GC has recently drawn increased attention being a precursor for novel carbon materials synthesis. Various amorphous and nanocrystalline carbon materials have been obtained with control of crystallinity and the  $sp^2/sp^3$  ratio using different high-pressure and temperature (HPHT) conditions. For instance, superstrong, transparent quenchable amorphous diamond at 40–50 GPa and  $\sim 1800$  K [6], superelastic compressed GC (with hardness of 26 GPa) at 25 GPa and 800–1000 °C [7], nanocrystalline diamond at 18–20 GPa and 2200–2300 K [8,9], nanocrystalline hexagonal diamond at 100 GPa and 400 °C (from type-II GC) [10], etc., have been synthesized. For these HPHT experiments of GC, the transitions usually take place through a nucleation process of tetrahedrally coordinated ( $sp^3$ -bonded) phases under sufficiently high pressures, akin to the graphite-diamond transition [11]. In contrast to the thermally activated transitions at high temperature in which the  $sp^3$ -bonded structures formed are quite stable, the transition in

cold-compressed GC (compressed at room temperature) may have a different mechanism.

While cold-compressed GC has been extensively studied using various techniques, our understanding of its transition still remains in a state of flux. *In situ* high-pressure x-ray Raman scattering experiments on GC at room temperature observed the gradual disappearance of the peak at  $\sim 285$  eV that corresponds to  $\pi$  bonding ( $1s$  to  $\pi^*$  excitation), suggesting an  $sp^2$ -to- $sp^3$  bonding transition in GC under high pressure [12]. Molecular dynamics and first-principles simulations also indicate that the  $sp^2$ -to- $sp^3$  bonding transition would occur when GC is under compression [13,14]. The pressure-induced transition in mechanical and optical properties of GC has also been reported. For instance, a GC sphere under quasiuniaxial compression by two diamond anvils showed superior strength, e.g., being able to sustain a stress difference of 70 GPa when the environmental hydrostatic pressure component is  $\sim 57$  GPa [12,15,16]. A uniaxially compressed GC sphere (bridged between two diamond anvils) was found to become translucent when the environmental pressure increased to above 33 GPa, while the GC spheres under quasihydrostatic compression remained opaque even up to 107 GPa [15,16]. However, there has been lacking a structural description for the various transitions in cold-compressed GC. In previous high-pressure x-ray diffraction (XRD) study of GC using Ne as the pressure medium, no evidence of a structural transition was observed up to 45.4 GPa [12]. On the other hand, the results of high-pressure Raman experiments remain controversial, e.g., substantial changes in Raman spectrum of cold-compressed GC have been observed in Refs. [15–17], but not in Ref. [18]. The inconsistency in various experiments hinders our understanding of the transition in cold-compressed GC. It is thus imperative to gain insights into the structural aspect of

\*zengzd@hpstar.ac.cn

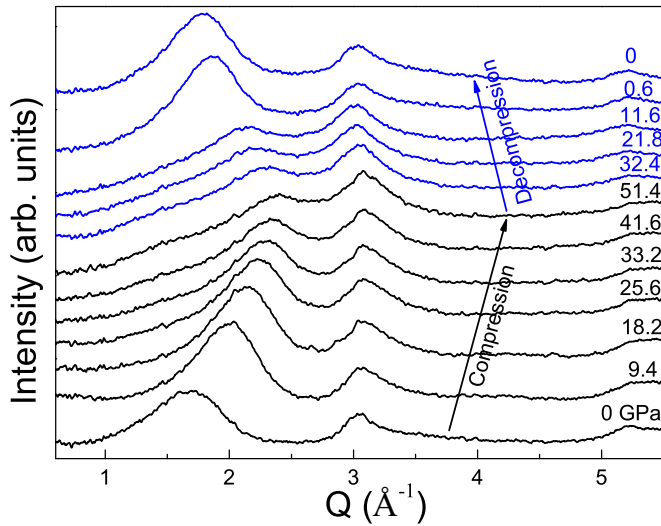


FIG. 1. *In situ* high-pressure XRD of GC. XRD patterns of GC at representative pressures during compression up to 51.4 GPa (black curves) and decompression to 0 GPa (blue curves). No pressure medium was used in the experiment in order to generate high deviatoric stress. The FDP and SDP correspond to the average interlayer distance of  $\sim 3.8$  Å and intralayer characteristic distance of  $\sim 2.05$  Å in GC at ambient pressure, respectively.

the pressure-induced transition in GC, especially because it is poised to be a new route for novel carbon materials discovery.

### II. EXPERIMENTAL DETAILS

GC is divided into type-I GC (synthesized below 2000 K) and type-II GC (synthesized above 2000 K) with different structures [5]. Type-I GC has a disordered layer structure, consisting of fragments of curved graphenelike layers (not graphene due to the presence of nonhexagonal rings, e.g., pentagons, heptagons, etc.), while type-II GC can be considered as mainly consisting of broken or imperfect fullerene-related nanoparticles, most of which are multilayered [2,5,19]. In this paper, GC refers to type-I GC unless specified. *In situ* high-pressure XRD experiments without pressure medium were performed at beamline 13 ID-D at the Advanced Photon Source (APS), Argonne National Laboratory (ANL). The x-ray (focused down to  $\sim 3$  μm) has a wavelength of 0.2952 Å. A MAR165 charge-coupled device detector was used for data collection, and the software DIOPTAS was used to integrate the two-dimensional images [20]. A symmetric diamond anvil cell (DAC) with the culet sizes of 300 μm was used to generate high pressure. GC samples (from Alfa Aesar) were loaded without pressure medium in order to introduce high shear stress. A tiny piece of Au foil was loaded along with the sample as the pressure standard. The pressure was determined using the equation of state of Au [21]. Background scattering from the diamond anvils was collected before loading the sample and subtracted to obtain XRD patterns of the sample.

### III. RESULTS AND DISCUSSION

Figure 1 shows the XRD patterns of the GC during compression up to 51.4 GPa and decompression to 0 GPa. The first diffraction peak [FDP, with a full width at half maximum

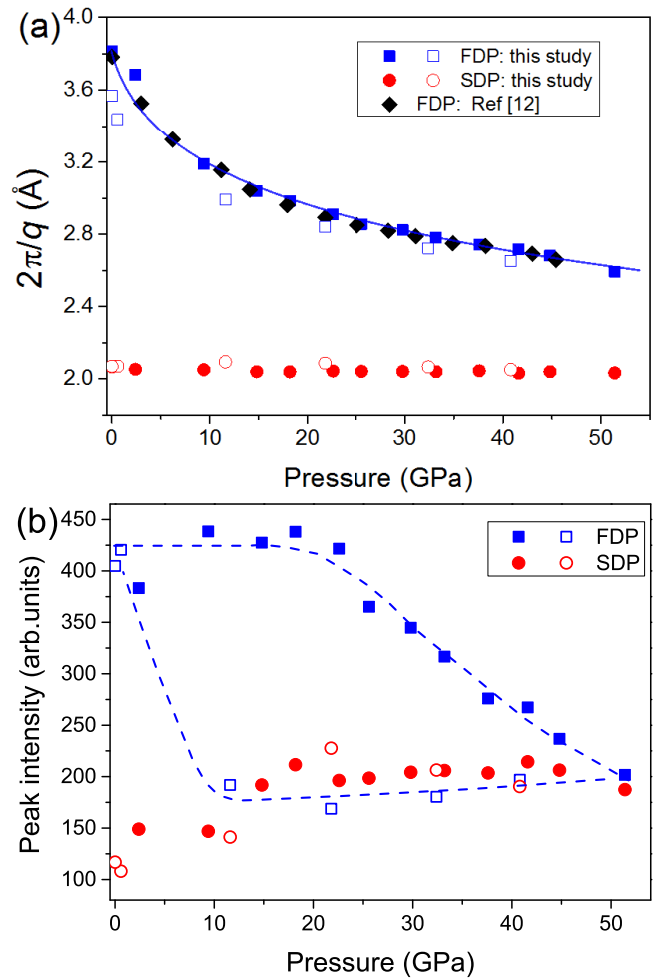


FIG. 2. Position (a) and intensity (b) of the FDP (square) and SDP (circle) of GC as functions of pressure during compression up to 51.4 GPa (solid symbols) and decompression (open symbols). The peak position and intensity were derived by fitting the diffraction peaks to Gaussian functions. The experimental data of GC from Ref. [12] (diamond) in which Ne was used as a hydrostatic pressure medium are also included for comparison. The pressure dependence of peak position in compression was fit to the third-order Birch-Murnaghan equation of state (solid line). Dashed line in (b) serves as a guide to the eye.

(FWHM) of  $\sim 0.6$  Å<sup>-1</sup>] and second diffraction peak (SDP, with a FWHM of  $\sim 0.3$  Å<sup>-1</sup>) are quite broad due to the highly disordered nature of GC. The FDP is well indicative of the presence of intermediate structure order in GC. The peak position and intensity of FDP and SDP were obtained by fitting the peaks to the Gaussian function (see Fig. 2). As mentioned before, GC consists of curved graphenelike layers. The interlayer distance (corresponding to FDP) shrinks smoothly to  $\sim 2.6$  Å (decreased by  $\sim 32\%$ ) when compressed to 51.4 GPa, consistent with previous high-pressure XRD results using a hydrostatic pressure medium (Ne) [12], as a consequence of the weak van der Waals force between the layers. Upon full decompression, the average interlayer distance ( $\sim 3.6$  Å) is slightly smaller than of starting material ( $\sim 3.8$  Å), indicating GC is  $\sim 5\%$  permanently densified if we

only consider the change of interlayer distance. Permanent pressure-induced densification (of  $\sim 10$  or  $\sim 15\%$ ) was also observed in the type-II GC after compression to  $\sim 35.5$  or 45 GPa [2,13].

Interestingly, in contrast to the continuous shift of the peak positions, the pressure dependence of the FDP intensity shows an apparent kink between 18.2 and 22.6 GPa [see Fig. 2(b)]. It remains almost constant below 18.2 GPa, whereas it drops continuously during further compression, with a total decrease of over 50% when compressed to 51.4 GPa, suggesting the drastic change of the intermediate structure order. By contrast, the peak intensity of the SDP does not show obvious change. The intensity of the FDP is dependent on the degree of ordering status (coherency) of the graphenelike layered structure in GC; thus its decrease implies that the layered structure is partially disturbed and the intermediate structural correlations become more disordered, e.g., due to the buckling and distortion of the graphenelike layers, and the transition to tetrahedral structure. The continuous decrease in peak intensity in a pressure range over 30 GPa suggests the structural transition is sluggish, and it has not finished even at the highest pressure of the experiment (51.4 GPa).

During decompression to 11.6 GPa, the FDP intensity does not show obvious changes, indicating a large hysteresis in the structural transition. This result implies that a high-energy barrier may exist between the high-pressure phase and the initial phase. Therefore, the more disordered high-pressure structure at 51.4 GPa can be maintained down to  $\sim 11.6$  GPa. Upon complete decompression, the intensity of FDP almost fully recovers, suggesting the original layered structure of GC is mostly restored in the recovered sample. As a consequence, the bonding and properties transitions under pressure are expected to be mainly reversible as well. This is consistent with the previous experimental observations, e.g., the  $\pi$ -bonding feature of GC that disappeared at 44.4 GPa reappeared upon decompression to 2.0 GPa; the translucent GC sphere under pressure (above 33 GPa) became opaque and broke when the pressure was removed [12,15,16]. It should be noted that for the type-II GC, the structure of the sample recovered from 13.1 GPa shows minor differences [2], while the sample recovered from 45 GPa or higher pressure is nanocrystalline graphite with preferred orientation [13]. It seems that type-I and type-II GC have quite different compression behavior, which also suggests the dominant role of atomic structure and its evolution in pressure-induced transitions in GC.

In addition to the *in situ* high-pressure experiments, first-principles calculations based on the Vienna *Ab initio* Simulation Package (VASP) were performed to derive detailed information of the atomic and electronic structure of GC under pressure [22]. *Ab initio* molecular-dynamics simulation was conducted to obtain GC by quenching liquid carbon with a fixed density of  $2.1 \text{ g/cm}^3$  from 5000 to 1000 K at a cooling rate of  $5 \times 10^{13} \text{ K/s}$ . A large structure model of GC with 1024 atoms was used in the simulation to obtain an accurate structural description of GC over a long structural range ( $r > 15 \text{ \AA}$ ) as well as reliable statistical structure factor [ $S(q)$ ] of GC. The simulations were carried out in a canonical ensemble (NVT) with each time step representing 2 fs. The temperature was controlled with the Nosé-Hoover thermostat [22]. The projector-augmented wave potential with a valence configura-

tion of  $2s2p$  and the generalized gradient approximation were used for C in the simulation [23]. We used the optB86b-vdW functional from the nonlocal exchange-correlation functions to account for the van der Waals correction [24]. To simulate hydrostatic compression of GC, the simulation box size was scaled at a rate of 0.995 each time, followed by conjugate gradient geometric optimization to achieve the minimum energy state of the structure. The high-resolution transmission microscopy (HRTEM) image of GC was simulated based on a multislice method using the atomic configuration of GC [25].

Figure 3 shows representative atomic configurations of GC during hydrostatic compression. The GC at ambient pressure (0.6 GPa) has a layered structure with most atoms bonded to three nearest-neighbor atoms in the same layer through  $sp^2$  covalent bonds [see Fig. 3(a)], which is consistent with the HRTEM image of GC at ambient pressure (see Supplemental Material [26]) [6]. The layers become more curved and densely packed at 19.8 GPa [Fig. 3(b)]. At 44.4 GPa, layer buckling and distortion become more obvious, and local tetrahedral structure (tetrahedral amorphous carbon) emerges by forming cross-linking  $sp^3$  bonds between adjacent layers [see Fig. 3(c)]. In fact, according to the high-pressure XRD results, the average interlayer distances are too long to form covalent bonds. For instance, the average interlayer distance is  $2.6 \text{ \AA}$  at 51.4 GPa, and it would only be reduced to  $2.35 \text{ \AA}$  even at 100 GPa estimated by extrapolation [see Fig. 2(a)]. For comparison, the length of  $sp^3$  bond in diamond is  $1.54 \text{ \AA}$ , and the upper limit of the C–C covalent bond length is usually set as  $1.80\text{--}1.85 \text{ \AA}$  in simulations [6,27]. However, the buckling and out-of-plane distortions of the graphenelike layers, especially the near-edge region of the layers, could reduce the local interlayer distance sharply, providing fertile sites for the formation of local tetrahedral structure and  $sp^3$  bonds. Figure 3(c) and Supplemental Material, Fig. S2 [26] show the distortion of the originally somewhat flat graphenelike layers under pressure and the tetrahedral structure formed in the severely distorted region. As structural transition proceeds with increasing pressure, the fraction of tetrahedral amorphous carbon and  $sp^3$  bonds increase, e.g.,  $sp^3$  fraction reaches 74% at 71.4 GPa [see Fig. 4(b)]. As a consequence, the original layered structure as a characteristic intermediate-range atomic order in the initial GC is mostly destroyed [see Fig. 3(d)]. It should be noted that a pure tetrahedral amorphous carbon (fully  $sp^3$  bonded) has not been obtained even up to 183 GPa (90%  $sp^3$ ) due to the lack of thermal activation.

The pressure-induced structural transition in GC is also clearly revealed in the calculated  $S(q)$  [see Fig. 4(a)]. The intensity of FDP of the  $S(q)$  decreases with increasing pressure due to the distortions of the graphenelike layers and the structural transition to tetrahedral amorphous carbon, agreeing with the high-pressure XRD results. The structural transition to tetrahedral amorphous carbon also explains the result that the SDP of the  $S(q)$  becomes obviously stronger at 57.6 GPa and higher pressure, because the tetrahedral amorphous carbon should have a diffraction peak around  $\sim 2.96 \text{ \AA}^{-1}$  at ambient conditions (similar to that of amorphous diamond) [6], which almost fully overlaps the SDP of GC. In addition, the tetrahedral amorphous carbon phase obtained at high pressure and room temperature is severely

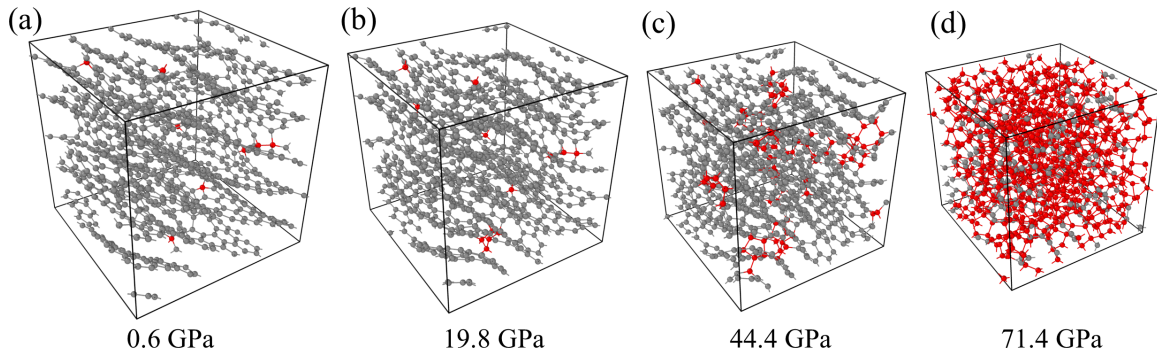


FIG. 3. Atomic configuration of GC at representative pressure 0.6 GPa (a), 19.8 GPa (b), 44.4 GPa (c), and 71.4 GPa (d) during hydrostatic compression obtained by first-principles calculations. The red spheres represent  $sp^3$ -bonded C atoms.

strained. Hence it is difficult to be preserved to ambient pressure, unlike the quenchable amorphous diamond obtained under high pressure and temperature [6]. The high strain introduced by the structural transition also explains why the  $sp^2$  bonds cannot be fully converted into  $sp^3$  bonds even

up to 183 GPa in the simulation without thermal-assisted relaxation. It should be noted that although the cooling rate in the simulation (to obtain GC structure) is much higher than that in the synthesis of GC, it provides a good structure model for GC, and the XRD and HRTEM data from the simulation match the experimental results quite well.

In contrast to our observation, in previous high-pressure XRD experiments using Ne as the hydrostatic pressure medium, GC shows no visible structural transition up to 45.4 GPa [12]. The different results indicate that shear stress should play an important role in this transition. To address the effect of shear stress, we further compared hydrostatic compression with uniaxial compression in the simulation. The results show that the  $sp^3$  fraction in GC starts to increase sharply at  $\sim 50$  GPa in hydrostatic compression, while it increases at  $\sim 35$  GPa in uniaxial compression [see Fig. 4(b)], indicating that the shear stress could significantly promote the structural transition in GC. The graphenelike layers in GC are expected to have superior out-of-plane flexibility similar to graphene. The uniaxial compression and large shear stress tend to make these layers reorient, deform, buckle, and slide, hence facilitate the structural transition. This can also help us interpret the previous experimental results that the pressure-induced transitions in Raman spectra, mechanical and optical properties of GC are susceptible to the presence of large shear stress [15,16].

During decompression, the  $sp^3$  fraction changes little down to  $\sim 10$  GPa for both hydrostatic and uniaxial stress, followed by substantial decrease in further decompression. The  $sp^3$  bonds with longer bond length (e.g., close to 1.8 Å) may be less stable in decompression, and may become nucleation sites for  $sp^2$ -bonded structure. The large hysteresis in the change of  $sp^3$  fraction in decompression is consistent with the XRD results, i.e., the intensity of FDP recovers when decompressed to below 11.6 GPa. It should be noted that the delayed transition pressure in simulation (compared with that in experiments) is caused by kinetics, since the modeling was conducted at 0 K and at an infinitely large compression rate, whereas the experiments were conducted at room temperature and at a moderate compression rate. In the structure recovered from hydrostatic compression, a small amount of  $sp^3$  bonds still exists ( $sp^3$  fraction  $\sim 5\%$ ), suggesting the pressure-induced transition in GC is not completely reversible.

As a structural and bonding-sensitive property, electrical conductivity has been extensively employed to study phase

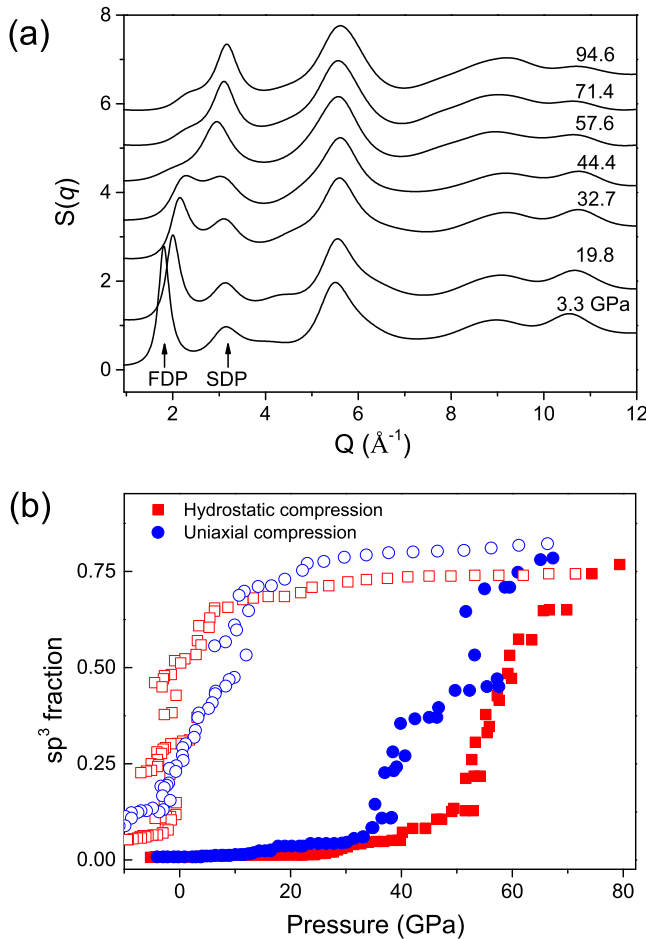


FIG. 4. (a) Structure factor  $[S(q)]$  of the GC as a function of pressure during hydrostatic compression. The  $S(q)$  was computed based on the radial distribution function following the Baxter-Dixon-Hutchinson factorization method [31]. (b) The fraction of  $sp^3$  bonds in GC as a function of pressure during hydrostatic compression (red squares) and uniaxial compression (blue circles), and decompression (open symbols).

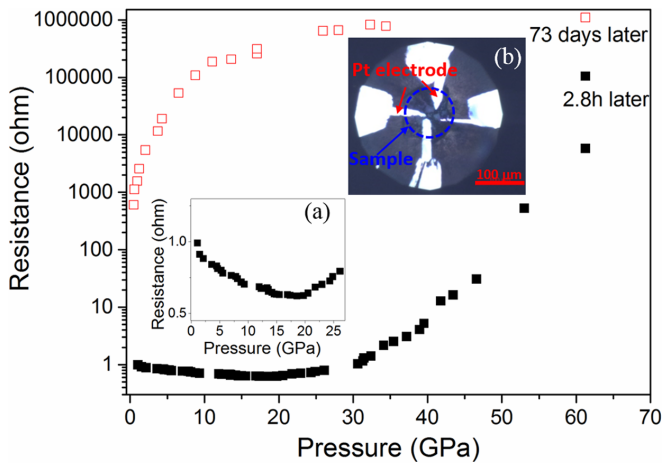


FIG. 5. Resistance of the GC sample as a function of pressure during compression (solid square) and decompression (open square). A log scale is used for resistance to reveal the change in low-resistance region. Inset a, zoomed-in plot of the resistance data below 27 GPa. Inset b, an optical microscope image of the sample (marked by the blue circle) with four Pt electrode probes for resistance measurement at 61.3 GPa. Ruby was used as the pressure calibrant. The scale bar represents 100  $\mu\text{m}$ .

transitions. The pressure dependence of the resistance of GC is obtained by the standard four-probe resistance measurement using a T301 stainless-steel–cubic boron nitride/epoxy mixture composite gasket (see Fig. 5, inset b). We measured the high-pressure resistance of GC up to 61 GPa without pressure medium at room temperature (see Fig. 5). The resistance decreases slightly with increasing pressure up to  $\sim 18.6$  GPa (similar to previous results measured up to  $\sim 13$  GPa in amorphous carbon) [28]. Above 18.6 GPa, the resistance increases by four orders of magnitude during further compression to 61.3 GPa (see Fig. 5 and inset a). The critical pressure ( $\sim 18.6$  GPa) of the transition coincides with that of the structural transition (18.2–22.6 GPa) in the high-pressure XRD experiments. The significant resistance increase in cold-compressed GC is in line with the formation of local tetrahedral structure under pressure. The electrical conductivity of GC is mainly contributed by  $\pi$ -electrons transfer in the layers. Therefore, the transition to the  $sp^3$ -bonded tetrahedral structure at the expense of  $\pi$  electrons and the integrity of the graphenelike layers would result in a remarkable increase in the resistivity of GC. Although the buckling and distortion in the graphenelike layers would also induce additional scattering for charge carriers and thus increase the resistance, the effect should be relatively minor (e.g., 20% strain would lead to resistance change of  $\sim 40\%$  for graphene wrinkles) [29]. The resistance reaches  $\sim 10^4 \Omega$  at 61.3 GPa (the highest pressure of the experiment), and still increases with time when the sample was kept at this pressure. The continuous change in resistance is consistent with the sluggish structural transition in GC, indicating that the transition has not finished at 61.3 GPa.

The change of resistance agrees well with the change in the calculated electronic density of states (EDOS) of GC under pressure (see Fig. 6). The EDOS of GC near Fermi surface remains almost the same in the low-pressure region,

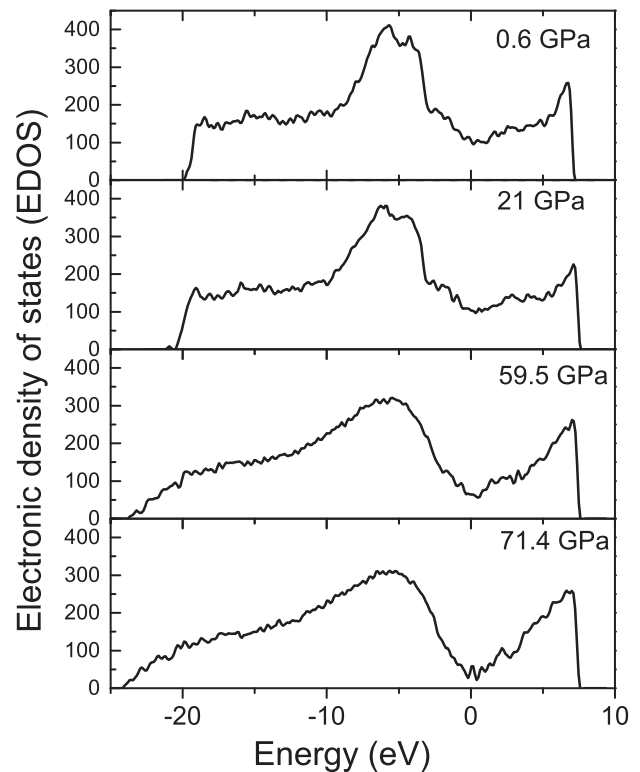


FIG. 6. Calculated EDOS of GC at different pressures during hydrostatic compression.

e.g., below 20 GPa, while it decreases remarkably at higher pressures. The change is also in line with the transition from  $sp^2$ -bonded layered structure to the  $sp^3$ -bonded tetrahedral network structure. It should be noted that a jump in the resistivity has also been observed in the shock-compressed GC at 45(5) GPa [30]. However, high temperature [around 1550(50) K] was inevitably involved in the shock-compression; hence caution should be exercised when comparing these results with our static cold-compression results.

Upon decompression to  $\sim 0.5$  GPa, the resistance drops over three orders of magnitude, suggesting that the structural and bonding transitions in GC are partially reversible. The resistance at 0.5 GPa is higher than that of the initial GC sample, which could result from the incomplete phase recovery of GC as suggested by simulation ( $\sim 5\%$  residual  $sp^3$  bonds), or defects and residual strain in the recovered GC. The increased resistance could also be partly attributed to the changed sample geometry (e.g., reduced sample thickness).

#### IV. SUMMARY

In summary, we used *in situ* high-pressure techniques and large-scale *ab initio* simulations to investigate the pressure-induced structural transition of GC at room temperature. The results reveal that the pressure-induced distortions in the graphenelike layers of GC effectively reduce the local interlayer distance, hence facilitate the transition of GC to a tetrahedral structure, which is partially reversible upon decompression. The transition to tetrahedral amorphous carbon is sluggish at room temperature, and it has not finished up to 61 GPa in our experiments. The critical pressure of the

transition could be substantially reduced by the presence of large shear stress. As a consequence of the structural transition, the resistance of GC also shows a partially reversible transition under pressure. Likewise, the previously reported property changes in cold-compressed GC, e.g., mechanical and optical properties, could be attributed to the structural transition observed in this study. Our work would thus provide a unified picture for the various transitions reported in cold-compressed glassy carbon.

#### ACKNOWLEDGMENTS

The authors thank Dr. Jianguo Wen for the help in TEM experiments. The authors acknowledge the financial support

of the National Natural Science Foundation of China (Grants No. U1530402 and No. 51871054) and the National Thousand Youth Talents Program in China. The XRD work was performed at the beamline 13-ID-D of GSECARS, APS, ANL. GSECARS is supported by the NSF (Grant No. EAR-1634415) and DOE (Grant No. DE-FG02-94ER14466). APS is supported by DOE-BES under Contract No. DE-AC02-06CH11357. Gas-loading system at GSECARS is partially supported by COMPRES under NSF Cooperative Agreement (Grant No. EAR 1606856). The TEM was performed at the Center for Nanoscale Materials at ANL, a DOE-BES Facility, supported under Contract No. DE-AC02-06CH11357 by UChicago Argonne, LLC.

- 
- [1] J. Bauer, A. Schroer, R. Schwaiger, and O. Kraft, *Nat. Mater.* **15**, 438 (2016).
- [2] Z. Zhao, E. F. Wang, H. Yan, Y. Kono, B. Wen, L. Bai, F. Shi, J. Zhang, C. Kenney-Benson, C. Park, Y. Wang, and G. Shen, *Nat. Commun.* **6**, 6212 (2015).
- [3] M. Vomero, E. Castagnola, F. Ciarpella, E. Maggiolini, N. Goshi, E. Zucchini, S. Carli, L. Fadiga, S. Kassegne, and D. Ricci, *Sci. Rep.* **7**, 40332 (2017).
- [4] J. J. VanDesarl, M. André, and R. Philippe, *Adv. Funct. Mater.* **25**, 78 (2015).
- [5] P. J. F. Harris, *Philos. Mag.* **84**, 3159 (2004).
- [6] Z. Zeng, L. Yang, Q. Zeng, H. Lou, H. Sheng, J. Wen, D. J. Miller, Y. Meng, W. Yang, W. L. Mao, and H.-k. Mao, *Nat. Commun.* **8**, 322 (2017).
- [7] M. Hu, J. He, Z. Zhao, T. A. Strobel, W. Hu, D. Yu, H. Sun, L. Liu, Z. Li, M. Ma, Y. Kono, J. Shu, H.-k. Mao, Y. Fei, G. Shen, Y. Wang, S. J. Juhl, J. Y. Huang, Z. Liu, B. Xu, and Y. Tian, *Sci. Adv.* **3**, e1603213 (2017).
- [8] L. Dubrovinsky, N. Dubrovinskaia, V. B. Prakapenka, and A. M. Abakumov, *Nat. Commun.* **3**, 1163 (2012).
- [9] H. Sumiya and T. Irifune, *J. Mater. Res.* **22**, 2345 (2007).
- [10] T. B. Shiell, D. G. McCulloch, J. E. Bradby, B. Haberl, R. Boehler, and D. R. McKenzie, *Sci. Rep.* **6**, 37232 (2016).
- [11] R. Z. Khaliullin, H. Eshet, T. D. Kühne, J. Behler, and M. Parrinello, *Nat. Mater.* **10**, 693 (2011).
- [12] Y. Lin, L. Zhang, H.-k. Mao, P. Chow, Y. Xiao, M. Baldini, J. Shu, and W. L. Mao, *Phys. Rev. Lett.* **107**, 175504 (2011).
- [13] T. B. Shiell, D. G. McCulloch, D. R. McKenzie, M. R. Field, B. Haberl, R. Boehler, B. A. Cook, C. de Tomas, I. Suarez-Martinez, N. A. Marks, and J. E. Bradby, *Phys. Rev. Lett.* **120**, 215701 (2018).
- [14] X. Jiang, C. Århammar, P. Liu, J. Zhao, and R. Ahuja, *Sci. Rep.* **3**, 1877 (2013).
- [15] M. Yao, J. Xiao, X. Fan, R. Liu, and B. Liu, *Appl. Phys. Lett.* **104**, 021916 (2014).
- [16] M. Yao, X. Fan, W. Zhang, Y. Bao, R. Liu, B. Sundqvist, and B. Liu, *Appl. Phys. Lett.* **111**, 101901 (2017).
- [17] A. F. Goncharov, *Zh. Eksp. Teor. Fiz.* **98**, 1824 (1990).
- [18] N. A. Solopova, N. Dubrovinskaia, and L. Dubrovinsky, *Appl. Phys. Lett.* **102**, 121909 (2013).
- [19] K. Jurkiewicz, S. Duber, H. E. Fischer, and A. Burian, *J. Appl. Crystallogr.* **50**, 36 (2017).
- [20] C. Prescher and V. B. Prakapenka, *High Press. Res.* **35**, 223 (2015).
- [21] O. L. Anderson, D. Isaak, and S. Yamamoto, *J. Appl. Phys.* **65**, 1534 (1989).
- [22] G. Kresse and J. Hafner, *Phys. Rev. B* **47**, 558 (1993).
- [23] P. E. Blöchl, *Phys. Rev. B* **50**, 17953 (1994).
- [24] M. Dixon and P. Hutchinson, *Mol. Phys.* **33**, 1663 (1977).
- [25] I. Lobato and D. Van Dyck, *Ultramicroscopy* **156**, 9 (2015).
- [26] See Supplemental Material at <http://link.aps.org/supplemental/10.1103/PhysRevMaterials.3.033608> for the experimental and simulated HRTEM images of GC, and thin slices of atomic configuration of GC in compression.
- [27] N. A. Marks, D. R. McKenzie, B. A. Pailthorpe, M. Bernasconi, and M. Parrinello, *Phys. Rev. B* **54**, 9703 (1996).
- [28] X. Li and H.-K. Mao, *Phys. Chem. Miner.* **21**, 1 (1994).
- [29] S. Deng and V. Berry, *Mater. Today* **19**, 197 (2016).
- [30] A. M. Molodets, A. A. Golyshev, A. N. Emel'yanov, Y. M. Shul'ga, and V. E. Fortov, *JETP Lett.* **99**, 237 (2014).
- [31] J. Klimeš, D. R. Bowler, and A. Michaelides, *Phys. Rev. B* **83**, 195131 (2011).